Comptes Rendus

Mécanique

Nguyen Thai Dung, Le Minh Thai, Tran Van Ke, Truong Thi Huong Huyen and Phung Van Minh

Nonlinear static bending analysis of microplates resting on imperfect two-parameter elastic foundations using modified couple stress theory

Short paper / *Note*

Nonlinear static bending analysis of microplates resting on imperfect two-parameter elastic foundations using modified couple stress theory

Nguyen Thai Dung⊕ *[a]*, **Le Minh Thai**⊕ *[a]*, **Tran Van Ke**⊕ *, [b],*
Truong Thi Huong Huyen⊕ *[b]* **and Phung Van Minh**⊕ *, [b]*

[a] Faculty of Special Equipment, Le Quy Don Technical University, 236 Hoang Quoc Viet Street, Hanoi 10000, Vietnam

[b] Faculty of Mechanical Engineering, Le Quy Don Technical University, 236 Hoang Quoc Viet Street, Hanoi 10000, Vietnam

E-mails: thaidung1966@gmail.com (N. Thai Dung), thailm@mta.edu.vn
(L. Minh Thai), tranvanke@lqdtu.edu.vn, tranke92@gmail.com (T. Van Ke),
huonghuyen.hvktqs@gmail.com (T. Thi Huong Huyen), minhpv@lqdtu.edu.vn,
minhpv.mta@gmail.com (P. Van Minh)

Abstract. The nonlinear static bending analysis of microplates resting on imperfect Pasternak elastic foundations is carried out in this paper. The finite element method based on the modified couple stress theory is used to derive the nonlinear finite element formulations. The present theory and mathematical model are validated by comparisons of this work's results with those of other reputable publications, which show a very good agreement. The influences of length-scale parameter, nonlinearity, elastic foundation parameters, imperfect foundations, and boundary conditions on the nonlinear static bending response of microplates are then explored. The computed data of this study is very intriguing, particularly the interaction of the microplate with the imperfect elastic foundation, and this helps us better understand the mechanical behavior of this structure.

Keywords. Nonlinearity, Static bending, Microplates, Modified couple stress, Imperfect elastic foundations.

1. Introduction

With the rapid advancement of science and technology, micro- and nano-sized structures have been utilized in a variety of sectors, including medical, pharmaceutical, optical, and

---

* Corresponding authors.

telecommunications, in recent decades [1–5]. As a result, researching and comprehending the mechanical reactions of these structures is crucial in the process of developing, producing, and integrating them into micromechanical systems. It is also tough to observe their reactions because of their micro- and nano-scales. The physico-mechanical response of microstructures started to get greater attention in the early 2000s. Fleck *et al.* [6] utilized dislocation theory to propose a rate-independent plasticity theory based on strain gradients. The accumulation of both randomly stored and geometrically required dislocations was thought to cause hardening. Lam *et al.* [7] carried out experiments on strain gradient elasticity, where the findings showed that in the elastic deformation of small-scale structures, the impact of elastic strain gradient was substantial. Then, a number of hypotheses have been developed to add on to the scientific knowledge of micro and nanoscale structures based on these significant and well-founded discoveries and studies [8–12].

For the study of mechanical behavior related to the microphone structure in general, some typical works can be listed as follows. For Timoshenko beams constructed of a functionally graded material, Asghari [13] proposed a size-dependent formulation (functionally graded material—FGM). The modified couple stress theory was used to derive the formulations. The modified couple stress theory is a non-classical continuous theory that can account for small-scale size effects in structural mechanics. Mohammad-Abadi and his co-workers [14] performed a vibration analysis of composite laminated beams on the micron scale using the modified couple stress theory. In the framework of strain gradient elasticity, the governing equation of motion of thin bending beams was investigated by Lazopoulos *et al.* [15]. The surface energy was used in conjunction with a simple linear strain gradient elastic theory. A variational approach was also employed to obtain the controlling beam equations and their boundary conditions. It turns out that new terms have been coined to emphasize the significance of the cross-section area in thin beam bending. Ma and colleagues [16] presented an improved variational formulation to simulate the microstructure-dependent Timoshenko beam model. It was based on Hamilton's concept and a modified coupled stress theory. Unlike the traditional theory, the new model included a material length-scale component and could account for the size effect. For third-order shear deformation functionally graded (FG) micro beams, a modified couple stress theory was developed by Salamat-talab *et al.* [17]. For the free vibration analysis of microplates, Ke and his team [18] proposed a Mindlin microplate model based on the modified couple stress theory. Based on a modified couple stress theory, Thai and Choi [19] introduced both size-dependent FG Kirchhoff and Mindlin plate models. Li *et al.* [20] used strain gradient elasticity theory to construct a size-dependent model for a bi-layered Kirchhoff microplate. The variational concept is used to obtain the governing equations and boundary conditions. Ansari and colleagues [21] introduced a Mindlin microplate model based on modified strain gradient elasticity to predict the axisymmetric bending, buckling, and free vibration properties of circular/annular microplates constructed of functionally graded materials. Sahmani and Ansari [22] predicted free vibration behavior of FGMs. The Mori–Tanaka homogenization approach assumes that the material characteristics of FGM microplates vary with thickness. Based on strain gradient elasticity theory, a non-classical higher-order shear deformable plate model with three material length-scale parameters is developed. Tho *et al.* [23] employed the finite element method (FEM) and an unique third-order shear deformation beam theory (TSDT) to predict the static bending and free vibration responses of rotating (around a fixed axis) piezoelectric nanobeams with geometrical imperfection and flexoelectric effects. Other publications [24–27] include some excellent work on mechanical responses of microstructures.

In actuality, both conventional and microscale structures may seem to have significant distortion. As a result, calculating the structure's nonlinear mechanical behavior is more complex. Moreover, nonlinear issues get more intriguing. The following are some publications dealing with

nonlinear calculations for microstructures. Ghayesh *et al.* [28] quantitatively investigated the nonlinear resonant dynamics of microbeams. The nonlinear partial differential equation controlling the system's motion was obtained using Hamilton's principle and the modified couple stress theory. The Galerkin approach, together with suitable eigenfunctions, was employed to discretize the nonlinear partial differential equation of motion into a series of nonlinear ordinary differential equations with linked components in order to make use of the available numerical methods. Asghari [29] used a modified version of the couple stress theory to derive the driving motion equations and boundary conditions for geometrically nonlinear microplates with variable forms. For the axisymmetrically nonlinear bending analysis of circular microplates under uniformly distributed transverse stresses, Wang *et al.* [30] offered a nonclassical Kirchhoff plate model. Jung and colleagues [31] developed a model for sigmoid functionally graded material (S-FGM) microplates based on the modified couple stress theory and first-order shear deformation. For imperfect functionally graded porous (FGP) cylindrical shells, Foroutan and Ahmadi [32] proposed semi-analytical and analytical methods for nonlinear static and dynamic buckling assessments. The structure is contained in a generalized nonlinear elastic foundation with nonlinear cubic stiffness and two Winkler–Pasternak parameters.

Furthermore, the mechanical interaction of the microstructure with elastic foundations is a fascinating issue in mechanical engineering. Structures, in fact, are often linked with completely solid or other soft components in the overall system. As a consequence, interactions between microstructures and elastic foundations have produced a slew of intriguing findings. Zhang *et al.* [33] proposed an efficient size-dependent plate model based on the strain gradient elasticity theory and a revised shear deformation theory to analyze the bending, buckling, and free vibration issues of FG microplates resting on an elastic foundation. Yang and his co-workers [34] investigated the buckling and post-buckling behaviors of microplates in a complex environment, taking into account an elastic foundation and hygro-thermal-electro-mechanical stresses. Li *et al.* [35] introduced an organic solar cell (OSC), which was considered the most potential third-generation solar energy application. The static bending and free vibration of the size-dependent OSC were extensively studied by using the modified strain gradient theory (MSGT) and the improved shear deformation plate theory. Gupta and Talha [36] studied the static and stability of a geometrically flawed FGM plate with a microstructural imperfection (porosity) on a Pasternak elastic base, based on higher-order shear and normal deformation theories. The effective material qualities of a material with porosity inclusion are expressed mathematically. A generic function models numerous geometric imperfections. An study of FGM rectangular plates bending in a thermal environment is presented by Bouderba [37]. Theoretical formulations use a refined shear deformation theory. The present theory's displacement field is based on nonlinear fluctuations in in-plane displacements throughout the plate's thickness. Thai and co-workers [38] utilized the finite element technique to model the mechanical, electrical, and polarization properties of piezoelectric nanoplates lying on elastic foundations and subjected to static stresses, taking into account the flexoelectric effect. Some remarkable works dealing with the nonlinear analysis of microstructures can be found in these works [31, 39–41].

As the outline above indicates, little study has been conducted on the nonlinear response of microplates resting on imperfect Pasternak's two-parameter elastic foundations. Hence, the purpose of this work is to improve our understanding of the mechanical behavior of microstructures in the context of nonlinear problems with imperfect elastic foundations.

This paper is organized as follows. Section 2 describes the nonlinear static bending of microplates resting on elastic foundations using finite element formulas. Section 3 discusses examples of verification and numerical findings. Section 4 presents the novel outcomes of the research.
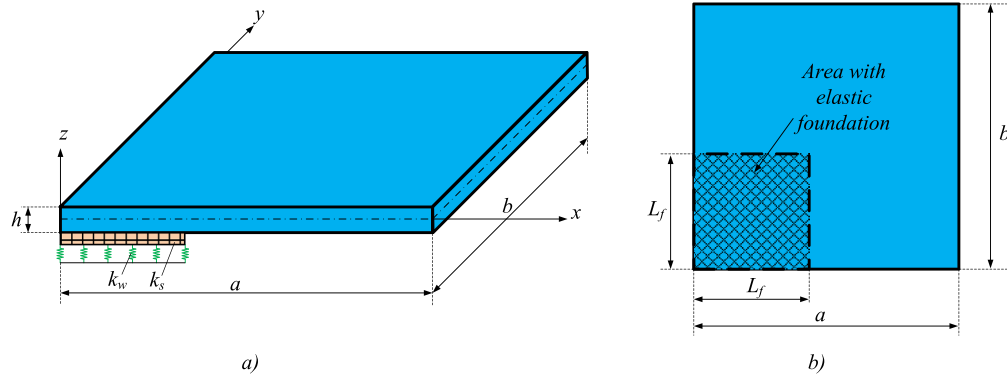
Figure 1. The model of a microplate resting on an elastic foundation. (a) General view; (b) top view.

2. Finite element formulations for nonlinear static bending of microplates resting on imperfect elastic foundations

Consider a homogeneous microplate with length a, width b, and thickness h, in which the plate is resting on an imperfect elastic medium with two parameters, the Winker spring k_w and the shear spring k_s, as shown in Figure 1.

The displacement field of each point in the microplate is expressed as follows using Mindlin's first-order shear deformation theory [42–44]:

$$\begin{cases} u = u_o + z \cdot \varphi_x \\ v = v_o + z \cdot \varphi_y \\ w = w_o \end{cases} \tag{1}$$

in which:

- The displacements in the x-, y-, and z-directions, respectively, are u, v, and w;
- The displacements of the point on the neutral surface in the x-, y-, and z-directions, respectively, are u_o, v_o, and w_o;
- The rotations of the cross-area around the y- and x-axes, respectively, are φ_x and φ_y.

The strain energy of the plate element is computed using the modified couple stress theory as follows [19]:

$$U_e = \int_{V_e} (\sigma_{ij}\varepsilon_{ij} + m_{ij} \cdot \chi_{ij}) \, dV_e, \tag{2}$$

where summation on repeated indices is implied; σ_{ij} are the components of the stress tensor; ε_{ij} are the components of the strain tensor; m_{ij} are the components of the deviatoric part of the symmetric couple stress tensor; and χ_{ij} are the components of the symmetric curvature tentors, which are defined as:

$$\chi_{ij} = \frac{1}{2}\left(\frac{\partial\theta_i}{\partial x_j} + \frac{\partial\theta_j}{\partial x_i}\right), \quad i, j = x, y, z \tag{3}$$

and θ_i are the rotation vector's components:

$$\theta_x = \frac{1}{2}\left(\frac{\partial w_0}{\partial y} - \varphi_y\right)$$

$$\theta_y = \frac{1}{2}\left(-\frac{\partial w_0}{\partial x} + \varphi_x\right) \tag{4}$$

$$\theta_z = \frac{1}{2}\left(\frac{\partial v}{\partial x} - \frac{\partial u}{\partial y} + z \cdot \frac{\partial\varphi_y}{\partial x} - z \cdot \frac{\partial\varphi_x}{\partial y}\right).$$

The nonlinear dependence of the bending strain on the displacement field is as follows [19]:

$$
\begin{cases}
\varepsilon_x = \dfrac{\partial u}{\partial x} + \dfrac{1}{2}\left(\dfrac{\partial w}{\partial x}\right)^2 = \dfrac{\partial u_o}{\partial x} + \dfrac{1}{2}\left(\dfrac{\partial w}{\partial x}\right)^2 + z \cdot \dfrac{\partial \varphi_x}{\partial x} \\[3mm]
\varepsilon_y = \dfrac{\partial v}{\partial y} + \dfrac{1}{2}\left(\dfrac{\partial w}{\partial y}\right)^2 = \dfrac{\partial v_o}{\partial y} + \dfrac{1}{2}\left(\dfrac{\partial w}{\partial y}\right)^2 + z \cdot \dfrac{\partial \varphi_y}{\partial y} \\[3mm]
\gamma_{xy} = \dfrac{\partial u}{\partial y} + \dfrac{\partial v}{\partial x} + \dfrac{\partial w}{\partial x} \cdot \dfrac{\partial w}{\partial y} = \left(\dfrac{\partial u_o}{\partial y} + \dfrac{\partial v_o}{\partial x}\right) + \dfrac{\partial w}{\partial x} \cdot \dfrac{\partial w}{\partial y} + z \cdot \left(\dfrac{\partial \varphi_x}{\partial y} + \dfrac{\partial \varphi_y}{\partial x}\right).
\end{cases}
\tag{5}
$$

Equation (5) is broken down into the following parts:

$$
\{\varepsilon_L\} = \left\{\dfrac{\partial u_o}{\partial x}, \dfrac{\partial v_o}{\partial y}, \dfrac{\partial u_o}{\partial y} + \dfrac{\partial v_o}{\partial x}\right\}^T; \quad
\{\varepsilon_{NL}\} = \left\{\dfrac{1}{2}\left(\dfrac{\partial w}{\partial x}\right)^2 \ \dfrac{1}{2}\left(\dfrac{\partial w}{\partial y}\right)^2 \ \dfrac{\partial w}{\partial x} \cdot \dfrac{\partial w}{\partial y}\right\}^T
$$

$$
\{\kappa\} = \left\{\dfrac{\partial \varphi_x}{\partial x}, \dfrac{\partial \varphi_y}{\partial y}, \dfrac{\partial \varphi_x}{\partial y} + \dfrac{\partial \varphi_y}{\partial x}\right\}^T.
$$

As a result, the bending strain may be expressed as:

$$
\{\varepsilon_b\} = \{\varepsilon_x, \varepsilon_y, \gamma_{xy}\}^T = \{\varepsilon_L\} + \{\varepsilon_{NL}\} + z \cdot \{\kappa\}.
\tag{6}
$$

The following equation defines the shear strain vector:

$$
\{\varepsilon_s\} = \begin{Bmatrix} \gamma_{xz} \\ \gamma_{yz} \end{Bmatrix} = \begin{Bmatrix} \dfrac{\partial u}{\partial z} + \dfrac{\partial w}{\partial x} \\[2mm] \dfrac{\partial v}{\partial z} + \dfrac{\partial w}{\partial y} \end{Bmatrix} = \left\{\varphi_x + \dfrac{\partial w}{\partial x} \ \ \varphi_y + \dfrac{\partial w}{\partial y}\right\}^T.
\tag{7}
$$

The symmetric curvature tentors' components are written as follows [19]:

$$
\{\chi_b\} = \left\{\chi_x \ \chi_y \ \chi_z \ \chi_{xy}\right\}^T
$$
$$
\{\chi_s\} = \left\{\chi_{yz} \ \chi_{zx}\right\}^T
\tag{8}
$$

in which

$$
\chi_x = \dfrac{1}{2}\left(\dfrac{\partial^2 w_0}{\partial y \partial x} - \dfrac{\partial \varphi_y}{\partial x}\right); \quad \chi_y = -\dfrac{1}{2}\left(\dfrac{\partial^2 w_0}{\partial x \partial y} - \dfrac{\partial \varphi_x}{\partial y}\right);
$$

$$
\chi_z = -\dfrac{1}{2}\left(-\dfrac{\partial \varphi_y}{\partial x} + \dfrac{\partial \varphi_x}{\partial y}\right); \quad \chi_{xy} = \dfrac{1}{4}\left(\dfrac{\partial^2 w_0}{\partial y^2} - \dfrac{\partial \varphi_y}{\partial y}\right) - \dfrac{1}{4}\left(\dfrac{\partial^2 w_0}{\partial x^2} - \dfrac{\partial \varphi_x}{\partial x}\right)
$$

$$
\chi_{yz} = -\dfrac{1}{4}z\left(-\dfrac{\partial^2 \varphi_y}{\partial x \partial y} + \dfrac{\partial^2 \varphi_x}{\partial y \partial y}\right) + \dfrac{1}{4}\left(\dfrac{\partial^2 v_0}{\partial x \partial y} - \dfrac{\partial^2 u_0}{\partial y \partial y}\right)
\tag{9}
$$

$$
\chi_{zx} = -\dfrac{1}{4}z\left(-\dfrac{\partial^2 \varphi_y}{\partial x \partial x} + \dfrac{\partial^2 \varphi_x}{\partial x \partial y}\right) + \dfrac{1}{4}\left(\dfrac{\partial^2 v_0}{\partial x \partial x} - \dfrac{\partial^2 u_0}{\partial x \partial y}\right).
$$

The following is a straightforward expression of (8).

$$
\{\chi_b\} = \dfrac{1}{4}\left\{\begin{array}{c} 2\left(\dfrac{\partial^2 w_0}{\partial y \partial x} - \dfrac{\partial \varphi_y}{\partial x}\right) \\[4mm] -2\left(\dfrac{\partial^2 w_0}{\partial x \partial y} - \dfrac{\partial \varphi_x}{\partial y}\right) \\[4mm] -2\left(-\dfrac{\partial \varphi_y}{\partial x} + \dfrac{\partial \varphi_x}{\partial y}\right) \\[4mm] \left(\dfrac{\partial^2 w_0}{\partial y^2} - \dfrac{\partial \varphi_y}{\partial y}\right) - \left(\dfrac{\partial^2 w_0}{\partial x^2} - \dfrac{\partial \varphi_x}{\partial x}\right) \end{array}\right\}; \quad \{\chi\}_s = \{\chi_{sm}\} + z \cdot \{\chi_{ss}\}
\tag{10}
$$

where

$$\{\chi_{sm}\} = \frac{1}{4}\left\{\begin{array}{c}\left(\dfrac{\partial^2 v_0}{\partial x \partial y} - \dfrac{\partial^2 u_0}{\partial y \partial y}\right) \\[2mm] \left(\dfrac{\partial^2 v_0}{\partial x \partial x} - \dfrac{\partial^2 u_0}{\partial x \partial y}\right)\end{array}\right\}; \quad \{\chi_{ss}\} = \frac{1}{4}\left\{\begin{array}{c}\dfrac{\partial^2 \varphi_y}{\partial x \partial y} - \dfrac{\partial^2 \varphi_x}{\partial y \partial y} \\[2mm] \dfrac{\partial^2 \varphi_y}{\partial x \partial x} - \dfrac{\partial^2 \varphi_x}{\partial y \partial x}\end{array}\right\}.$$

The following is how the stress fields are computed:

  • *The normal stress field*:

$$\{\sigma_b\} = \left\{\begin{array}{c}\sigma_x \\ \sigma_y \\ \tau_{xy}\end{array}\right\} = [D_b] \cdot \left\{\begin{array}{c}\varepsilon_x \\ \varepsilon_y \\ \gamma_{xy}\end{array}\right\} = [D_b]\{\varepsilon_L\} + [D_b]\{\varepsilon_{NL}\} + z \cdot [D_b] \cdot \{\kappa\} \tag{11}$$

in which

$$[D_b] = \frac{E}{1-\mu^2}\begin{bmatrix}1 & \mu & 0 \\ \mu & 1 & 0 \\ 0 & 0 & \dfrac{1-\mu}{2}\end{bmatrix}$$

is the material matrix; E and μ are the Young's modulus and Poisson's ratio, respectively.

  • *The shear stress field:*

$$\{\tau\} = [D_s]\{\varepsilon_s\} \tag{12}$$

in which

$$[D_s] = \begin{bmatrix}G & 0 \\ 0 & G\end{bmatrix}; \quad G = \frac{E}{2(1+\mu)}.$$

  • *The components of the deviatoric part of the symmetric couple stress tensor [19]*:

$$\{m\} = [D_o]\{\chi_b\}; \quad \{n\} = [D_{os}]\{\chi_s\}, \tag{13}$$

where

$$[D_0] = \frac{E \cdot l_o^2}{1+\mu}\begin{bmatrix}1 & 0 & 0 & 0 \\ 0 & 1 & 0 & 0 \\ 0 & 0 & 1 & 0 \\ 0 & 0 & 0 & 1\end{bmatrix} \quad \text{and} \quad [D_{os}] = \frac{E \cdot l_o^2}{2(1+\mu)}\begin{bmatrix}1 & 0 \\ 0 & 1\end{bmatrix}$$

are the material matrices; l_o is the length-scale parameter, which depends on materials.

The strain energy is now expressed as follows:

$$U_e = \frac{1}{2}\int_{S_e}\left(\begin{array}{c}\left\{\begin{array}{c}\{\varepsilon_L\}+\{\varepsilon_{NL}\} \\ \{\kappa\} \\ \{\varepsilon_s\}\end{array}\right\}^T \begin{bmatrix}[A] & [B] & [0]_{3x2} \\ [B] & [D] & [0]_{3x2} \\ [0]_{2x3} & [0]_{2x3} & [A]\end{bmatrix}\left\{\begin{array}{c}\{\varepsilon_L\}+\{\varepsilon_{NL}\} \\ \{\kappa\} \\ \{\varepsilon_s\}\end{array}\right\} \\[6mm] + \left\{\begin{array}{c}\{\chi_b\} \\ \{\chi_{sb}\} \\ \{\chi_{ss}\}\end{array}\right\}^T \begin{bmatrix}[C] & [0]_{4x2} & [0]_{4x2} \\ [0]_{2x4} & [Y] & [0]_{2x4} \\ [0]_{2x4} & [0]_{2x4} & [X]\end{bmatrix}\left\{\begin{array}{c}\{\chi_b\} \\ \{\chi_{sb}\} \\ \{\chi_{ss}\}\end{array}\right\}\end{array}\right)\,dx\,dy, \tag{14}$$

where

$$([A],[B],[D]) = \int_{-h/2}^{h/2}[D_b](1,z,z^2)\,dz; \quad [A] = k_{cr}\int_{-h/2}^{h/2}[D_s]\,dz;$$

$$[C] = \int_{-h/2}^{h/2}[D_o]\,dz; \quad ([Y],[X]) = \int_{-h/2}^{h/2}[D_{os}](1,z)\,dz, \tag{15}$$

in which $k_{cr} = 5/6$ is the shear correction factor.

In this study, a four-node quadrilateral element is used, with each node having five degrees of freedom, as shown in Figure 2.

$$\{q_e\} = \{\{q_1\} \ \{q_2\} \ \{q_3\} \ \{q_4\}\}^T; \quad \{q_i\} = \{u_{0i} \ v_{0i} \ w_{0i} \ \varphi_{xi} \ \varphi_{yi}\}^T.$$

The Lagrange shape functions and the element displacement vector are then used to extend the components of the strain tensor and the components of the symmetric curvature tensors as follows:

$$\{\varepsilon_N\} = [B_1^L]\{q_e\}; \quad \{\varepsilon_{NL}\} = [B_1^{NL}]\{q_e\}; \quad \{\kappa\} = [B_2]\{q_e\}; \quad \{\varepsilon_s\} = [B_3]\{q_e\};$$
$$\{\chi_b\} = [B_4]\{q_e\}; \quad \{\chi_{sm}\} = [B_5]\{q_e\}; \quad \{\chi_{ss}\} = [B_6]\{q_e\},$$
(16)

in which

$$B_1^L = \sum_{i=1}^{4} \begin{bmatrix} \dfrac{\partial N_i}{\partial x} & 0 & 0 & 0 & 0 \\ 0 & \dfrac{\partial N_i}{\partial y} & 0 & 0 & 0 \\ \dfrac{\partial N_i}{\partial y} & \dfrac{\partial N_i}{\partial x} & 0 & 0 & 0 \end{bmatrix}; \quad [B_1^{NL}] = \frac{1}{2} \begin{bmatrix} \dfrac{\partial w}{\partial x} & 0 \\ 0 & \dfrac{\partial w}{\partial y} \\ \dfrac{\partial w}{\partial y} & \dfrac{\partial w}{\partial x} \end{bmatrix} \sum_{i=1}^{4} \begin{bmatrix} 0 & 0 & \dfrac{\partial N_i}{\partial x} & 0 & 0 \\ 0 & 0 & \dfrac{\partial N_i}{\partial y} & 0 & 0 \end{bmatrix}$$

$$[B_2] = \sum_{i=1}^{4} \begin{bmatrix} 0 & 0 & 0 & \dfrac{\partial N_i}{\partial x} & 0 \\ 0 & 0 & 0 & 0 & \dfrac{\partial N_i}{\partial y} \\ 0 & 0 & 0 & \dfrac{\partial N_i}{\partial y} & \dfrac{\partial N_i}{\partial x} \end{bmatrix}; \quad [B_3] = \sum_{i=1}^{4} \begin{bmatrix} 0 & 0 & \dfrac{\partial N_i}{\partial x} & 1 & 0 \\ 0 & 0 & \dfrac{\partial N_i}{\partial y} & 0 & 1 \end{bmatrix}$$

$$[B_4] = \frac{1}{4} \sum_{i=1}^{4} \begin{bmatrix} 0 & 0 & 2\dfrac{\partial^2 N_i}{\partial y \partial x} & 0 & -2\dfrac{\partial N_i}{\partial x} \\ 0 & 0 & -2\dfrac{\partial^2 N_i}{\partial x \partial y} & 2\dfrac{\partial N_i}{\partial y} & 0 \\ 0 & 0 & 0 & -2\dfrac{\partial N_i}{\partial y} & 2\dfrac{\partial N_i}{\partial x} \\ 0 & 0 & \dfrac{\partial^2 N_i}{\partial y^2} - \dfrac{\partial^2 N_i}{\partial x^2} & \dfrac{\partial N_i}{\partial x} & -\dfrac{\partial N_i}{\partial y} \end{bmatrix}$$

$$[B_5] = \sum_{i=1}^{4} \frac{1}{4} \begin{bmatrix} -\dfrac{\partial^2 N_i}{\partial y \partial y} & \dfrac{\partial^2 N_i}{\partial x \partial y} & 0 & 0 & 0 \\ -\dfrac{\partial^2 N_i}{\partial x \partial y} & \dfrac{\partial^2 N_i}{\partial x \partial x} & 0 & 0 & 0 \end{bmatrix}; \quad [B_6] = \sum_{i=1}^{4} \frac{1}{4} \begin{bmatrix} 0 & 0 & 0 & -\dfrac{\partial^2 N_i}{\partial y \partial y} & \dfrac{\partial^2 N_i}{\partial x \partial y} \\ 0 & 0 & 0 & -\dfrac{\partial^2 N_i}{\partial y \partial x} & \dfrac{\partial^2 N_i}{\partial x \partial x} \end{bmatrix},$$

where N_i ($i = 1$–4) denotes the Lagrange shape functions, which are written as:

$$N_1 = \tfrac{1}{4}(1-\xi)(1-\eta); \quad N_2 = \tfrac{1}{4}(1+\xi)(1-\eta)$$
$$N_3 = \tfrac{1}{4}(1+\xi)(1+\eta); \quad N_4 = \tfrac{1}{4}(1-\xi)(1+\eta).$$

• ξ and η are the natural coordinates (see Figure 2).

Equation (14), when substituted, yields:

$$U_e = \frac{1}{2} \cdot \{q_e\}^T \cdot \left[\int_{S_e} \left(\begin{bmatrix} [B_1^L] + [B_1^{NL}] \\ [B_2] \\ [B_3] \end{bmatrix}^T \begin{bmatrix} [A] & [B] & [0]_{3x2} \\ [B] & [D] & [0]_{3x2} \\ [0]_{2x3} & [0]_{2x3} & [A] \end{bmatrix} \begin{bmatrix} [B_1^L] + [B_1^{NL}] \\ [B_2] \\ [B_3] \end{bmatrix} + \begin{bmatrix} [B_4] \\ [B_5] \\ [B_6] \end{bmatrix}^T \begin{bmatrix} [C] & [0]_{4x2} & [0]_{4x2} \\ [0]_{2x4} & [Y] & [0]_{2x4} \\ [0]_{2x4} & [0]_{2x4} & [X] \end{bmatrix} \begin{bmatrix} [B_4] \\ [B_5] \\ [B_6] \end{bmatrix} \right) \mathrm{d}x\,\mathrm{d}y \right] \cdot \{q_e\}. \quad (17)$$

As a consequence, the element stiffness matrix for the microplate element without accounting for elastic foundations is as follows:
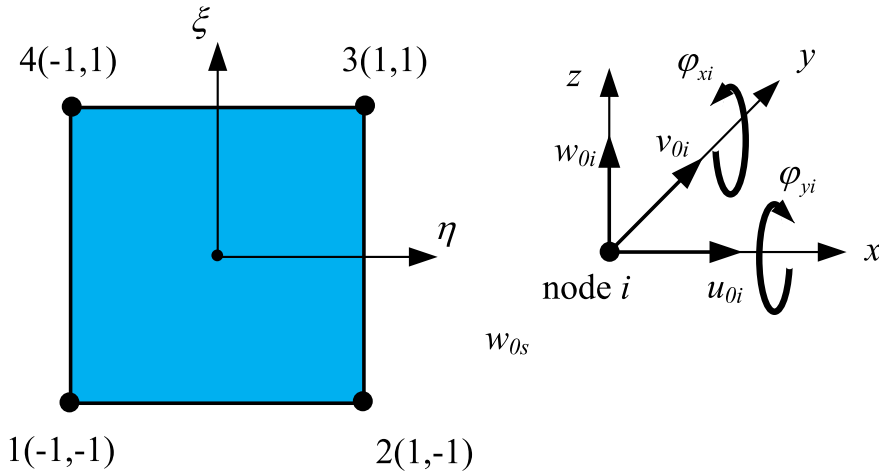
$$[K_e^1] = [K_e^L] + [K_e^{NL}]$$
(18)

Figure 2. A four-node quadrilateral element [45, 46].

where matrices of linear and nonlinear element stiffness are written as follows:

$$
[K_e^L] = \int_{S_e} \left(\begin{bmatrix} [B_1^L] \\ [B_2] \\ [B_3] \end{bmatrix}^T \begin{bmatrix} [A] & [B] & [0]_{3x2} \\ [B] & [D] & [0]_{3x2} \\ [0]_{2x3} & [0]_{2x3} & [A] \end{bmatrix} \begin{bmatrix} [B_1^L] \\ [B_2] \\ [B_3] \end{bmatrix} \right.
$$
$$
\left. + \begin{bmatrix} [B_4] \\ [B_5] \\ [B_6] \end{bmatrix}^T \begin{bmatrix} [C] & [0]_{4x2} & [0]_{4x2} \\ [0]_{2x4} & [Y] & [0]_{2x4} \\ [0]_{2x4} & [0]_{2x4} & [X] \end{bmatrix} \begin{bmatrix} [B_4] \\ [B_5] \\ [B_6] \end{bmatrix} \right) \, \mathrm{d}x\,\mathrm{d}y \tag{19}
$$

$$
[K_e^{NL}] = \int_{S_e} \left(\begin{matrix} [B_1^L]^T \cdot [B] \cdot [B_1^{NL}] + [B_1^{NL}]^T \cdot [B] \cdot [B_1^L] \\ + [B_1^{NL}]^T \cdot [A] \cdot [B_1^{NL}] + [B_1^{NL}]^T \cdot [B] \cdot [B_2] \\ + [B_2]^T \cdot [B] \cdot [B_1^{NL}] \end{matrix} \right) \, \mathrm{d}x\,\mathrm{d}y.
$$

The elastic foundation's strain energy in a plate element is computed as follows:

$$
U_e^f = \frac{1}{2} \int_{S_e} \left(k_w w^2 + k_s \left(\left(\frac{\partial w}{\partial x} \right)^T \left(\frac{\partial w}{\partial x} \right) + \left(\frac{\partial w}{\partial y} \right)^T \left(\frac{\partial w}{\partial y} \right) \right) \right) \mathrm{d}x\,\mathrm{d}y \tag{20}
$$

in which k_w and k_s are the Winker spring and shear spring, respectively.

The extra stiffness of the elastic foundation is produced as follows by expanding similar to the preceding expressions:

$$
[K_e^f] = \int_{S_e} \left(k_w [N_w]^T [N_w] + k_s \left([N_{w,x}]^T [N_{w,x}] + [N_{w,y}]^T [N_{w,y}] \right) \right) \mathrm{d}x\,\mathrm{d}y, \tag{21}
$$

where

$$
[N_w] = \sum_1^4 [0,0,N_i,0,0]; \quad [N_{w,x}] = \sum_1^4 \left[0,0,\frac{\partial N_i}{\partial x},0,0 \right]; \quad [N_{w,y}] = \sum_1^4 \left[0,0,\frac{\partial N_i}{\partial y},0,0 \right]. \tag{22}
$$

As a result, the plate element's stiffness matrix, which includes the elastic foundation, is defined as follows:

$$
[K_e] = [K_e^1] + [K_e^f]. \tag{23}
$$

Then, in order to compute the element's nodal force vector, the following equation of work done by external forces is used.

$$
A_e = \int_{S_e} \{u\}^T \{f\} \, \mathrm{d}S_e, \tag{24}
$$

where $\{u\}^T = \{u_0 \ v_0 \ w_0 \ \varphi_x \ \varphi_y\} = \{q_e\}^T \cdot [N]^T; \{f\} = \{0 \ 0 \ q(x,y) \ 0 \ 0\}^T.$

Equation (24) now becomes:

$$A_e = \{q_e\}^T \int_{S_e} [N]^T \{f\} \, dx \, dy. \tag{25}$$

Thus, one gets:

$$\{F_e\} = \int_{S_e} ([N]^T \{f\}) \, dx \, dy. \tag{26}$$

The static equilibrium equation for the entire microplate is derived after assembling the components of element matrices and vectors:

$$\left(\underbrace{[K^f] + [K^L]}_{\text{linear part}} + \underbrace{[K^{NL}]}_{\text{nonlinear part}} \right) \cdot \{Q\} = \{F\}. \tag{27}$$

To solve (27), the Newton–Raphson method is conducted [47,48]. For the convenience of explaining the solution, Equation (27) is abbreviated as follows:

$$K(Q) \cdot Q = F. \tag{28}$$

Supposing the value of the displacement is determined in step i indicated by Q^i, the following Taylor expansion to first order is employed to determine displacements in the subsequent step (Q^{i+1}):

$$K(Q^{i+1}) \approx K(Q^i) + K_T^i(Q^i)\Delta Q^i = F, \tag{29}$$

where $K_T^i(Q^i) = (\partial K/\partial Q)^i$ contains a Jacobian matrix, often referred to as the tangent stiffness matrix, and ΔQ^i displacement increment. The displacement increment ΔQ^i may be calculated using (29).

$$K_T^i(Q^i)\Delta Q^i = F - K(Q^i). \tag{30}$$

Now that Equation (30) has been used to get the displacement increment ΔQ^i, the displacement in the next step Q^{i+1} is determined as follows:

$$Q^{i+1} = Q^i + \Delta Q^i. \tag{31}$$

Equation (31)'s solution does not fulfill the precise roots of nonlinear (28). At this point, an unbalanced force will exist:

$$R^{i+1} = F - K(Q^{i+1}). \tag{32}$$

This procedure is continued until the unbalanced force equals the specified value; at that point, Q^{i+1} is acknowledged as a solution to the nonlinear (28). To calculate this stationary time, $\delta^{\text{conv}} \leq \delta_0$ performs a comparison of the convergence parameter, where δ^{conv} is calculated as:

$$\delta^{\text{conv}} = \frac{\sum_{j=1}^n (R_j^{i+1})^2}{1 + \sum_{j=1}^n (F_j)^2} \tag{33}$$

and $\delta_0 = 10^{-4}$ is an acceptable value.

3. Numerical results and discussions

This paper makes use of a variety of boundary conditions. The definition includes the following boundary conditions for simplicity of follow-up: C for clamped support, S for simple support, and F for a free edge.

3.1. *Verification examples*

At first, two examples are introduced to verify the present theory and the MATLAB-based calculation program that will be used to examine the effect of geometrical and material parameters on
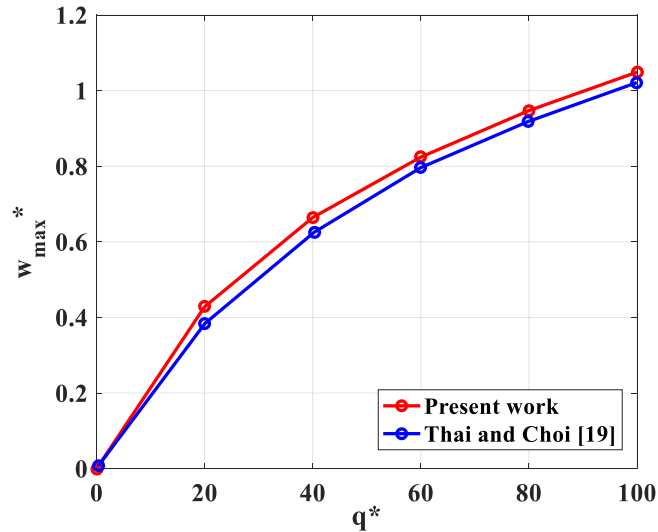
Figure 3. Comparative non-dimensional maximum deflections.

the mechanical responses of microplates resting on two-parameter elastic foundations. The first is an issue with the nonlinear static bending response of microplates without elastic foundations, while the second one is a problem with the linear static bending response of microplates resting on Pasternak elastic foundations.

Example 1. Consider a fully simply supported square homogeneous microplate with the following dimensions and material properties [19]: $h = 17.6 \times 10^{-6}$ m, $a = b = 20h$, $l_0 = 0.2h$, Young's modulus $E = 1.44$ GPa, Poisson's ratio $\mu = 0.38$, and two elastic foundation parameters, $k_w = k_s = 0$. The load is applied in a sinusoidally dispersed manner as follows [19]:

$$q(x, y) = q_o \sin\left(\frac{\pi}{2}x\right)\sin\left(\frac{\pi}{2}y\right) \tag{34}$$

in which q_o can be found in the equation of normalized force as follows:

$$q^* = \frac{q_o a^4}{Eh^4}. \tag{35}$$

The non-dimensional maximum deflection for verification examples is defined as:

$$w_{\max}^* = \frac{100Eh^3}{q_o a^4} w\left(\frac{a}{2}, \frac{b}{2}\right). \tag{36}$$

Figure 3 presents the comparative non-dimensional maximum deflections between this work and Thai and Choi [19].

Example 2. To validate the calculation program for the microplate with an elastic foundation, the maximum deflection of the microplate with an elastic medium in the case of a linear problem is examined. Consider a SSSS square homogeneous microplate [33], where $h = 17.6 \times 10^{-6}$ m, $a = b = kxh$ (k is open), $l_0 = 0.2h$, Young's modulus $E = 380$ GPa, Poisson's ratio $\mu = 0.3$. The sinusoidally distributed load is expressed in (34) and (35). Two non-dimensional elastic foundation parameters are normalized as follows:

$$k_w^* = \frac{k_w a^2 b^2}{D}; \quad k_s^* = \frac{k_s ab}{D} \tag{37}$$
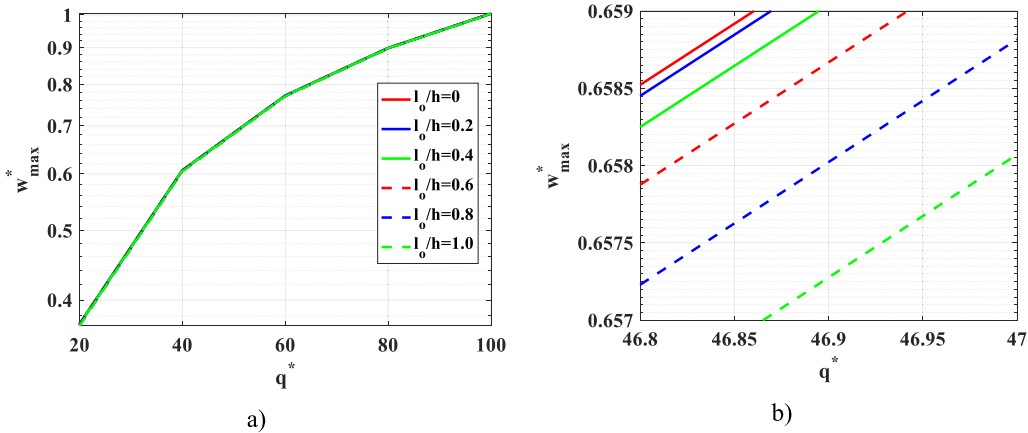
in which $D = Eh^3/12(1 - \mu^2)$.

Figure 4. The non-dimensional maximum deflection depends on the length-scale parameter; SSSS; $a/h = 20$; $k_w^* = k_s^* = 5$.

It can be observed that the computed results are in very excellent agreement, as shown in Figure 3 and Table 1. As a result, the proposed theory and mathematical model have been proven correct.

3.2. *Parameter investigations*

Now, the influence of geometrical and material parameters of microplates resting on elastic foundations are being explored. Consider a square microplate with the following parameters [19]: $h = 17.6 \times 10^{-6}$ m, $a = b = kxh$ (k can be changed), length-scale parameter l_0, Young's modulus $E = 14.4$ GPa, Poisson's ratio $\mu = 0.38$. The sinusoidally distributed load is expressed in (34) and (35). Two non-dimensional elastic foundation parameters are normalized as presented in (37). Non-dimensional deflection of microplates is defined as:

$$w* = \frac{w(x, y)}{h}. \tag{38}$$

3.2.1. *Effect of length-scale parameter*

The length-scale parameter plays a significant role in the mechanical responses of the microstructures. Therefore, this subsection first explores the influence of this coefficient on the nonlinear static bending of microplates. Herein, the SSSS microplate is considered. The effect of the length-scale parameter is shown in Figure 4. Note that all the detailed geometrical and material coefficients are also presented in these figures.

As demonstrated in Figure 4, the length-scale parameter has a small impact on the microplate's nonlinear deflection response. The variation in maximum deflection for each external load amount is insignificant. For microstructures, the deflection decreases as the length-scale parameter l_o is increased.

3.2.2. *Effect of the nonlinearity*

Nonlinearity is examined in this section. The normalized force has a range of values from 0 to 200. The following is a definition of the distinction between nonlinear and linear dimensionless deflections:

$$w^{\text{diff}} = |w_{\text{max}}^* \text{ (linear)} - w_{\text{max}}^* \text{ (nonlinear)}|. \tag{39}$$

Figure 5 shows the deflection responses for both linear and nonlinear situations.

Table 1. Comparison of non-dimensional maximum deflection of the microplate resting on the two-parameter elastic foundation

| k_w^*	$a/h = 20$								$a/h = 100$							
	$k_s^* = 0$		$k_s^* = 10$		$k_s^* = 20$		$k_s^* = 50$		$k_s^* = 0$		$k_s^* = 10$		$k_s^* = 20$		$k_s^* = 50$	
	Zhang *et al.* [33]	This work	Zhang *et al.* [33]	This work	Zhang *et al.* [33]	This work	Zhang *et al.* [33]	This work	Zhang *et al.* [33]	This work	Zhang *et al.* [33]	This work	Zhang *et al.* [33]	This work	Zhang *et al.* [33]	This work
0	0.2738	0.2742	0.2420	0.2432	0.2170	0.2181	0.1658	0.1665	0.2719	0.2731	0.2406	0.2420	0.2158	0.2171	0.1650	0.1669
10	0.2702	0.2712	0.2393	0.2401	0.2146	0.2163	0.1645	0.1652	0.2684	0.2697	0.2378	0.2397	0.2136	0.2145	0.1637	0.1646
20	0.2667	0.2679	0.2366	0.2379	0.2125	0.2132	0.1632	0.1643	0.2649	0.2656	0.2351	0.2366	0.2114	0.2126	0.1624	0.1637
50	0.2567	0.2577	0.2286	0.2298	0.2061	0.2076	0.1594	0.1599	0.2551	0.2574	0.2273	0.2288	0.2051	0.2068	0.1587	0.1598
100	0.2417	0.2453	0.2168	0.2185	0.1965	0.1985	0.1536	0.1548	0.2403	0.2422	0.2155	0.2169	0.1954	0.1991	0.1529	0.1540
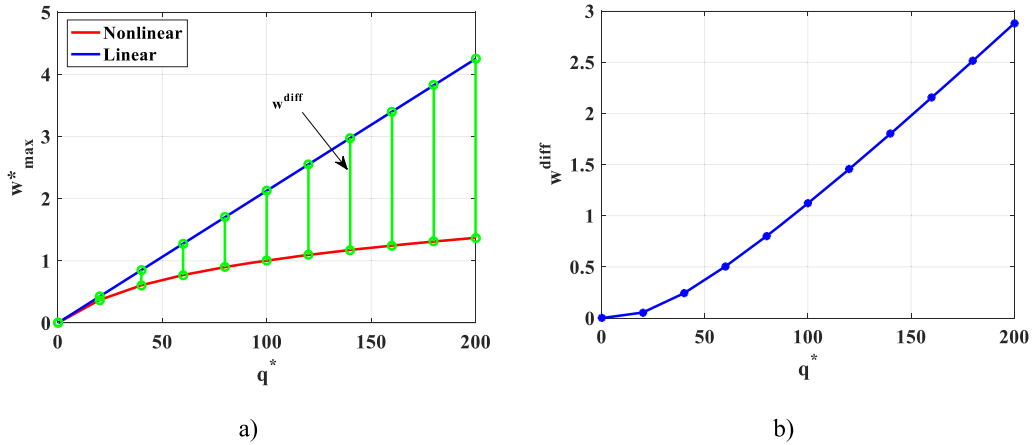
Figure 5. The distinction between nonlinear and linear non-dimensional maximum deflections; SSSS; $a/h = 20$, $l_o/h = 0.2$; $\overline{k}_w = \overline{k}_p = 5$.
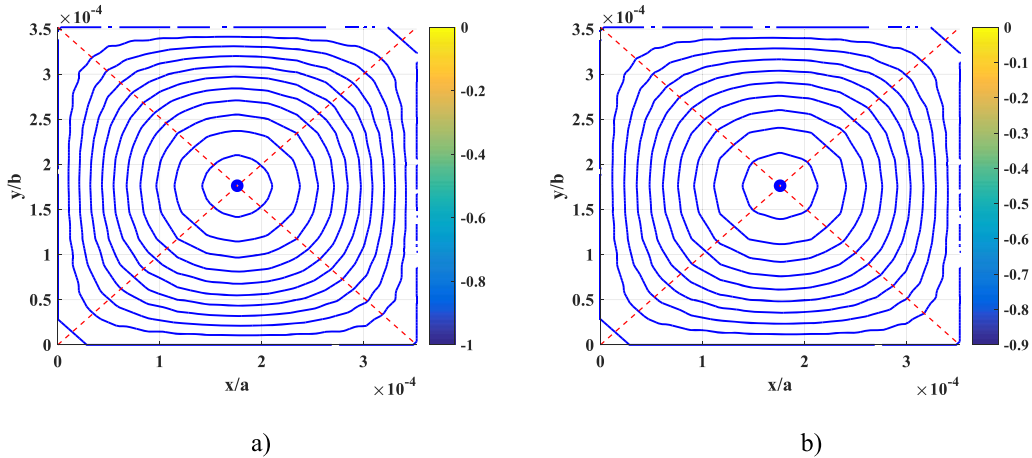

Figure 6. The dependence of the nonlinear deflection w^* of microplates on elastic foundation parameters; SSSS; $a/h = 20$; $l_o/h = 0.2$; $q^* = 100$; (a) $k_w^* = k_s^* = 5$; (b) $k_w^* = k_s^* = 10$.

It can be seen from Figure 5 that there is a significant difference between nonlinear and linear problems. The difference is minimal when the load is modest. This discrepancy gets increasingly obvious as the load intensity rises, and it rises quickly as the load intensity rises. This is another fascinating aspect of the nonlinear issue. The numerical results in this nonlinear case more accurately describe the response of microplates when the load is increased. Closely monitoring the mechanical reaction of conventional structures, as well as nano- and micro-sized structures, which is extremely challenging to measure, is also an intriguing aspect of the nonlinear analysis problem.

3.2.3. *Effect of elastic foundation parameters*

To continue, the effect of elastic foundation parameters is examined. Let $k_w^* = 5$ and k_s^* obtains the values of 0 to 10. In contrast, $k_s^* = 5$ and $k_w^* = 0 \div 10$ are also considered. The non-dimensional maximum deflection is shown in Figure 6. Note that in this subsection, a full elastic foundation is considered.
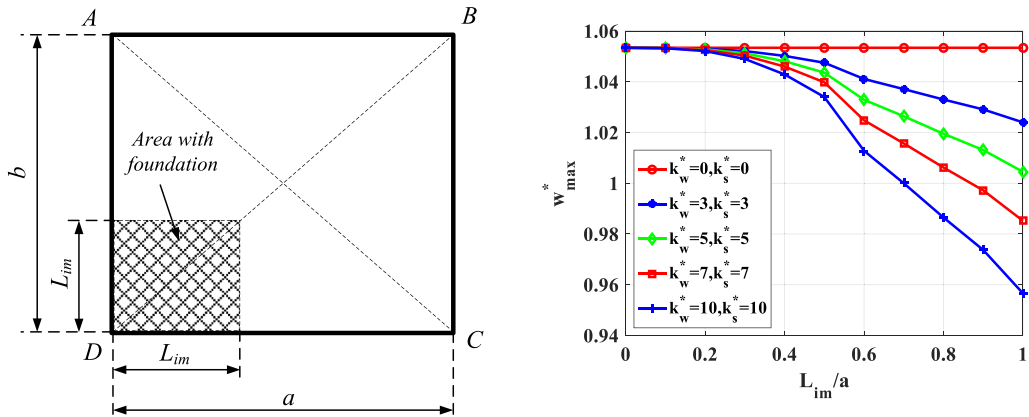
Figure 7. The dependence of the non-dimensional maximum deflection w^* of microplate elastic foundation distribution; SSSS; $a/h = 20$; $l_o/h = 0.2$; $q^* = 100$.

Table 2. The dependence of the non-dimensional maximum deflection $w^*_{\max}$ on elastic foundation parameters; SSSS; $a/h = 20$; $q^* = 100$

		Non-dimensional maximum deflection $w^*_{\max}$			
	l_o/h	$k^*_s = 0$	$k^*_s = 3$	$k^*_s = 5$	$k^*_s = 7$	$k^*_s = 10$
	0	1.0510	1.0230	1.0045	0.9861	0.9589
	0.2	1.0510	1.0230	1.0045	0.9861	0.9589
$k^*_w = 5$	0.4	1.0510	1.0230	1.0045	0.9861	0.9588
	0.6	1.0510	1.0229	1.0044	0.9860	0.9586
	0.8	1.0508	1.0227	1.0042	0.9857	0.9584
	1.0	1.0505	1.0224	1.0038	0.9854	0.9580
	l_o/h	$k^*_w = 0$	$k^*_w = 3$	$k^*_w = 5$	$k^*_w = 7$	$k^*_w = 10$
	0	1.0069	1.0055	1.0045	1.0036	1.0022
	0.2	1.0068	1.0054	1.0045	1.0036	1.0022
$k^*_s = 5$	0.4	1.0068	1.0054	1.0045	1.0035	1.0021
	0.6	1.0067	1.0053	1.0044	1.0034	1.0020
	0.8	1.0065	1.0051	1.0042	1.0032	1.0018
	1.0	1.0062	1.0048	1.0038	1.0029	1.0015

The stiffness of the elastic foundation has a considerable impact on the static nonlinear response of the microplate, as shown in Table 2 and Figure 6. The overall stiffness of the structure increases as the foundation stiffness increases. As a consequence, the deflection of the microplate is minimized.

3.2.4. *Effect of imperfect elastic foundation*

Now, this subsection performs an exploration of the effect of an imperfect elastic foundation. An SSSS square microplate resting on a corner square area of elastic foundation is presented in Figure 7. The dependence of non-dimensional maximum deflection of microplates on the square area of elastic foundation is presented in Figure 8.

Figure 8 shows various kinds of imperfect elastic foundations and the associated deflection shapes of microplates to better understand how the area of the foundation affects the nonlinear deflection response of microplates.
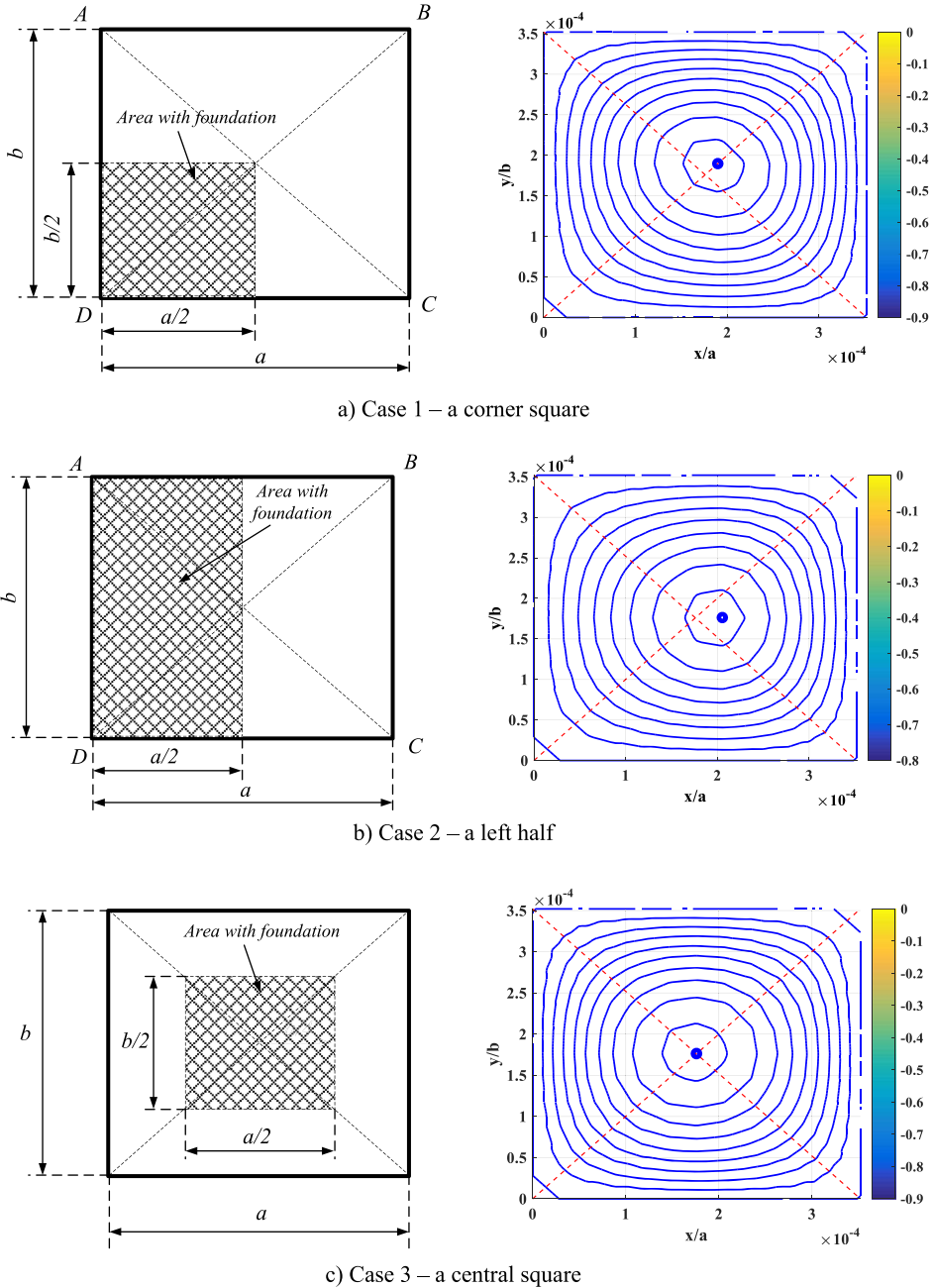
a) Case 1 – a corner square

b) Case 2 – a left half

c) Case 3 – a central square

Figure 8. Continued on next page.

The uneven elastic foundation distribution has a relatively substantial influence on the non-linear static response of the microplates, as shown in Figures 7 and 8. The apparent deflection diminishes as the width L_{im} of the elastic foundation distribution region increases in Figure 7. The reason for this is that when the distribution area of the foundation increases, the structure's stiffness is reinforced by the foundation's stiffness. When the structure and the elastic foundation
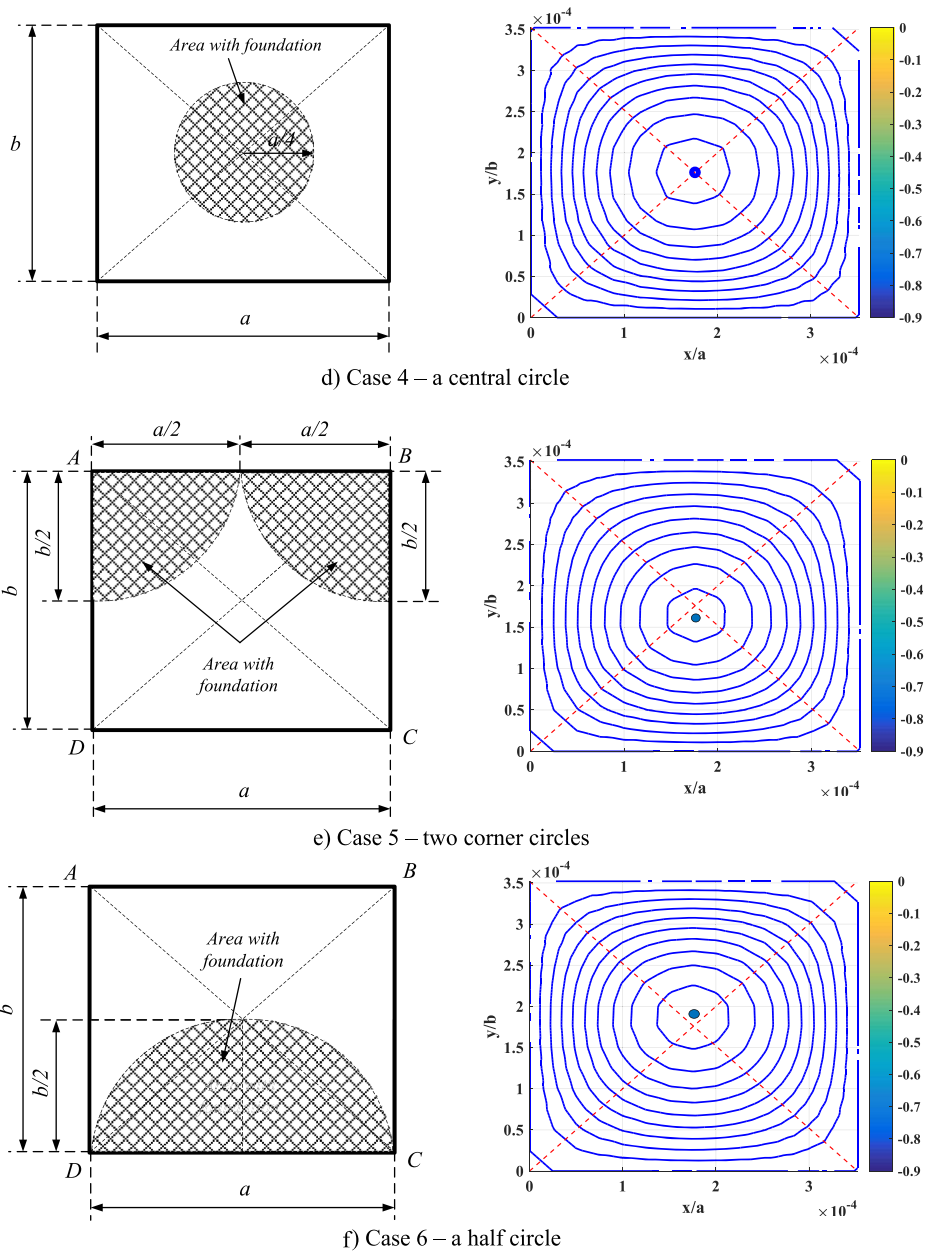
d) Case 4 – a central circle

e) Case 5 – two corner circles

f) Case 6 – a half circle

Figure 8 (cont.). The deformation of microplates depends on imperfect two-parameter elastic foundation SSSS; $a/h = 20$; $l_o/h = 0.2$; $q^* = 100$; $k_w^* = k_s^* = 30$.

are symmetrically centered, the point with the highest deflection coincides with the center of symmetry, as shown in Figure 8. The deformation shape of the microplate tends to be symmetrical along an axis when the plate and foundation are spread symmetrically about that axis. When there is no central symmetry, the center of deflection tends to migrate to the region with no elastic foundation, i.e. the region with lower stiffness.
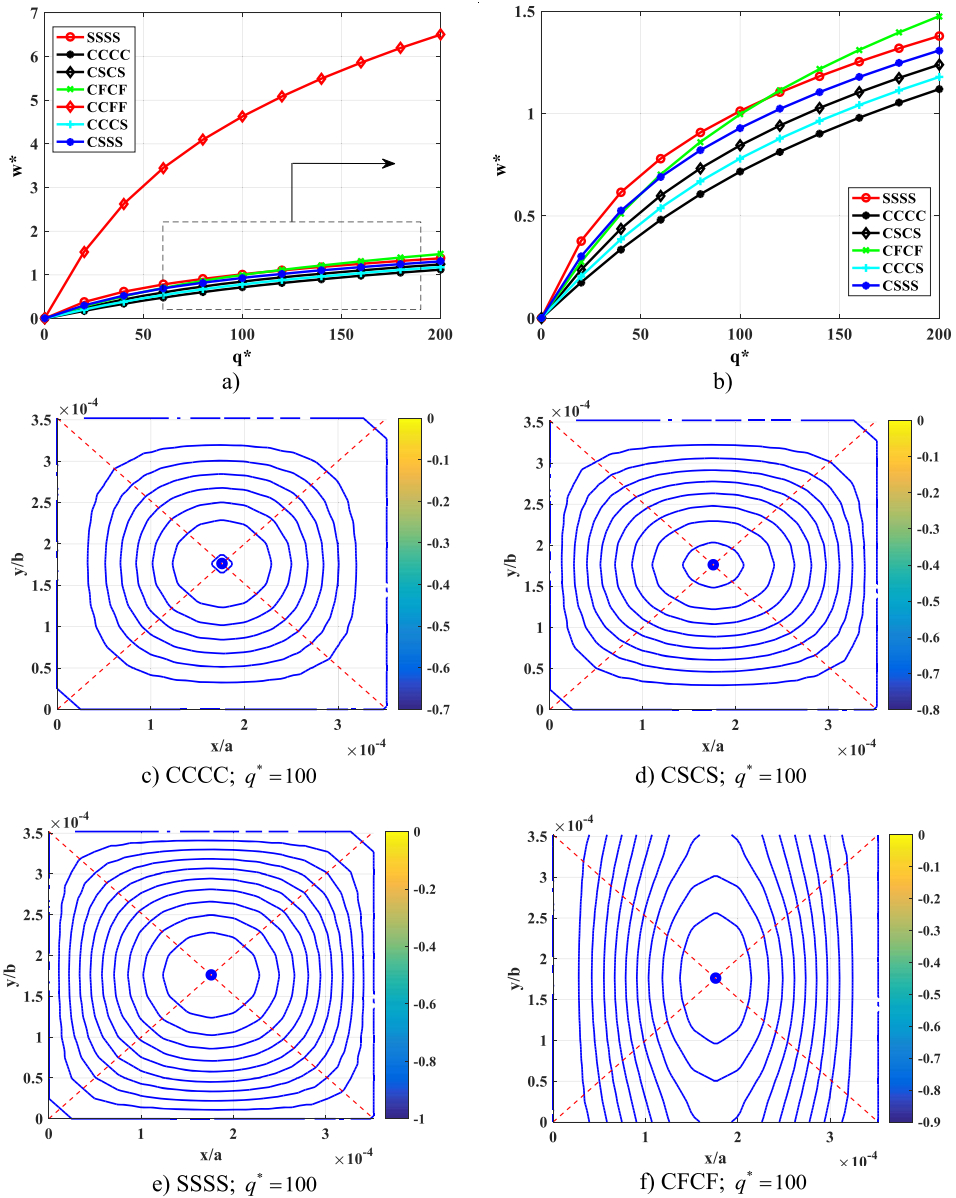
a)

b)

c) CCCC; $q^* = 100$

d) CSCS; $q^* = 100$

e) SSSS; $q^* = 100$

f) CFCF; $q^* = 100$

Figure 9. Continued on next page.

3.2.5. *Effect of boundary conditions*

Finally, the impact of boundary conditions on microplate nonlinear static bending is investigated. Boundary conditions are calculated in three different ways (CCCC, CSCS, and SSSS).

The accompanying Figure 9 depicts the mechanical behavior of microplates as a function of boundary conditions. It should be noted that in this subsection, a full elastic foundation is considered. The reader may observe from Figure 9 that boundary circumstances have a significant impact on the nonlinear static bending of microplates. Because the structure stiffens as the plate gets more self-enforced, the maximum deflection is lowered. The plate with the
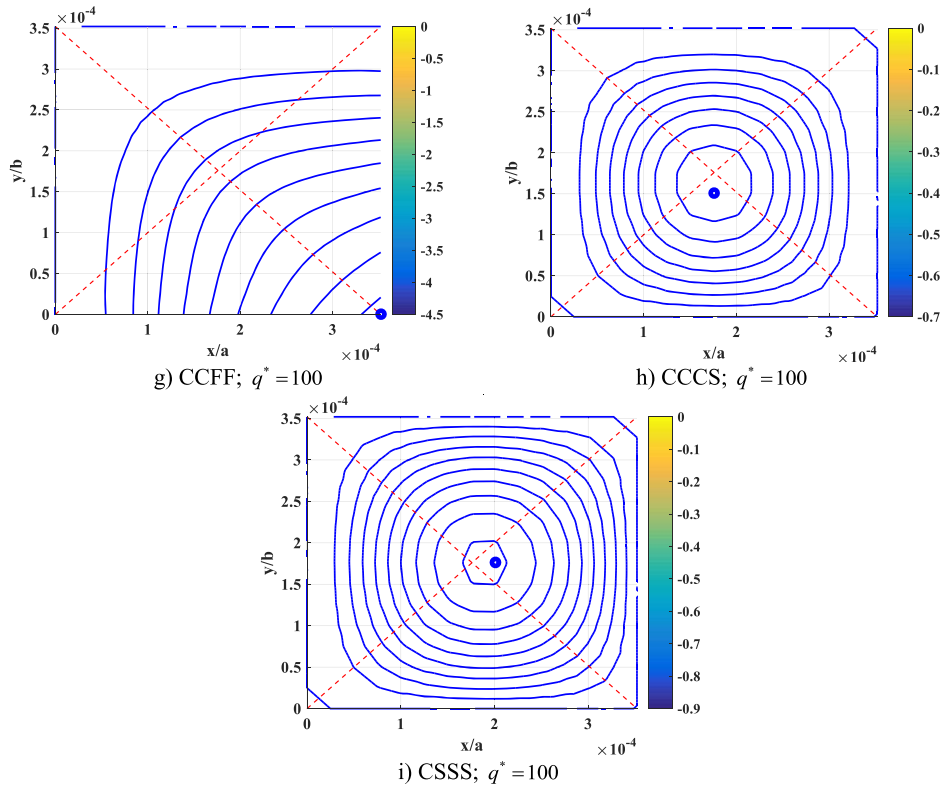
g) CCFF; $q^* = 100$
h) CCCS; $q^* = 100$

i) CSSS; $q^* = 100$

Figure 9. The deformation of microplates depends on boundary conditions; $a/h = 20$; $l_o/h = 0.2$; $k_w^* = k_s^* = 5$.

boundary condition CCCC is the stiffest, followed by the CCCS plate, and finally the CCFF plate. Furthermore, the structure and elastic foundation in all three boundary conditions have a symmetrical distribution, thus the point of greatest deflection is at the center of the plate.

4. Conclusions

The nonlinear static bending responses of microplates resting on imperfect Pasternak's elastic foundations are investigated in this paper. The modified couple stress theory is used to derive the finite element formulations. Comparisons of the findings of these studies to those of other trustworthy research reveal a high degree of agreement. The following are some novel points.

- The length-scale parameter l_o has a trivial effect on the static nonlinear response of microplates, as shown in the numerical findings and comments part of this parameter survey section. In contrast to the linear problem, where this parameter has a significant influence on the nonlinear static response of microplates, this is not the case here.
- The distinction between nonlinear and linear issues is crucial. When the load is light, the difference is negligible. As the load intensity increases, the difference becomes more noticeable, and it increases fast. This is another intriguing element of the nonlinear problem.
- The nonlinear response of the microplate is greatly influenced by the stiffness as well as the dispersion of the imperfect elastic foundation. The foundation stiffness rises, leading

to increase in the structure's total stiffness. As a consequence, the deflection is minimized. The distribution of an unsatisfactory elastic foundation is also seen in the distorted forms of the plate under external loads. The distorted shape of the plate is likewise symmetrical since the structure tends to be aligned and the dimensions are symmetrical. For asymmetrically organized imperfect foundations, the greatest deflection point tends to migrate to the position of low stiffness.

- The maximum deflection is reduced when the structure stiffens as the plate becomes more self-enforced. The stiffest plate is the one with the boundary condition CCCC, followed by the CSCS plate, and lastly, the SSSS plate.

Moreover, the numerical findings presented in this study are noteworthy since they add to our understanding of the nonlinear behavior of microplates. It is very important to note that the mechanical models, finite element formulas, and programming in the MATLAB environment that have been developed as a result of this study will serve as the foundation for further research and development of more complex problems related to microstructures, such as eigenvibration and dynamics problems involving large deformations.

Conflicts of interest

The author declares that there are no conflicts of interest regarding the publication of this paper.

Acknowledgment

References

[1] I. S. Chronakis, "Micro- and nano-fibers by electrospinning technology: processing, properties, and applications", in *Micromanufacturing Engineering and Technology*, William Andrew, Oxford, UK, 2nd ed., 2015, p. 513-548.

[2] L. Tsakalakos, "Application of micro- and nanotechnology in photovoltaics", *Compr. Renew. Energy* **1** (2012), p. 515-531.

[3] N. Hao, J. Lu, R. Hua, W.-W. Zhao, K. Wang, "New micro- and nanotechnologies for electrochemical biosensor development", in *Advanced Biosensors for Health Care Applications*, Elsevier, Amsterdam, Netherlands, 2019, p. 279-313.

[4] G. L. Cotè, L. H. V. Wang, S. Rastegar, "Biomedical optics and lasers", in *Introduction to Biomedical Engineering*, Academic Press, Cambridge, MA, USA, 2011, p. 1111-1173.

[5] M. Nasrollahzadeh, Z. Issaabadi, M. Sajjadi, S. M. Sajadi, M. Atarod, "Types of nanostructures", *Interface Sci. Technol.* **28** (2019), p. 29-80.

[6] N. A. Fleck, G. M. Muller, M. F. Ashby, J. W. Hutchinson, "Strain gradient plasticity: Theory and experiment", *Acta Metall. Mater.* **42** (1994), no. 2, p. 475-487.

[7] D. C. C. Lam, F. Yang, A. C. M. Chong, J. Wang, P. Tong, "Experiments and theory in strain gradient elasticity", *J. Mech. Phys. Solids* **51** (2003), no. 8, p. 1477-1508.

[8] M. A. Neto, A. Amaro, L. Roseiro, J. Cirne, R. Leal, in *Finite Element Method for Plates/Shells BT — Engineering Computation of Structures: The Finite Element Method* (M. A. Neto, A. Amaro, L. Roseiro, J. Cirne, R. Leal, eds.), Springer International Publishing, Cham, 2015, p. 195-232.

[9] J. N. Reddy, "Nonlocal theories for bending, buckling and vibration of beams", *Int. J. Eng. Sci.* **45** (2007), no. 2, p. 288-307.

[10] F. Yang, A. C. M. Chong, D. C. C. Lam, P. Tong, "Couple stress based strain gradient theory for elasticity", *Int. J. Solids Struct.* **39** (2002), no. 10, p. 2731-2743.

[11] M. Jirásek, "Nonlocal theories in continuum mechanics", *Acta Polytech.* **44** (2004), p. 16-34.

[12] C. W. Lim, G. Zhang, J. N. Reddy, "A higher-order nonlocal elasticity and strain gradient theory and its applications in wave propagation", *J. Mech. Phys. Solids* **78** (2015), p. 298-313.

[13] M. Asghari, M. Rahaeifard, M. H. Kahrobaiyan, M. T. Ahmadian, "The modified couple stress functionally graded Timoshenko beam formulation", *Mater. Des.* **32** (2011), no. 3, p. 1435-1443.

[14] M. Mohammad-Abadi, A. R. Daneshmehr, "Modified couple stress theory applied to dynamic analysis of composite laminated beams by considering different beam theories", *Int. J. Eng. Sci.* **87** (2015), p. 83-102.

[15] A. K. Lazopoulos, "Dynamic response of thin strain gradient elastic beams", *Int. J. Mech. Sci.* **58** (2012), no. 1, p. 27-33.

[16] H. M. Ma, X.-L. Gao, J. N. Reddy, "A microstructure-dependent Timoshenko beam model based on a modified couple stress theory", *J. Mech. Phys. Solids* **56** (2008), no. 12, p. 3379-3391.

[17] M. Salamat-talab, A. Nateghi, J. Torabi, "Static and dynamic analysis of third-order shear deformation FG micro beam based on modified couple stress theory", *Int. J. Mech. Sci.* **57** (2012), no. 1, p. 63-73.

[18] L.-L. Ke, Y.-S. Wang, J. Yang, S. Kitipornchai, "Free vibration of size-dependent Mindlin microplates based on the modified couple stress theory", *J. Sound Vib.* **331** (2012), no. 1, p. 94-106.

[19] H.-T. Thai, D.-H. Choi, "Size-dependent functionally graded Kirchhoff and Mindlin plate models based on a modified couple stress theory", *Compos. Struct.* **95** (2013), p. 142-153.

[20] A. Li, S. Zhou, S. Zhou, B. Wang, "A size-dependent model for bi-layered Kirchhoff micro-plate based on strain gradient elasticity theory", *Compos. Struct.* **113** (2014), no. 1, p. 272-280.

[21] R. Ansari, R. Gholami, M. Faghih Shojaei, V. Mohammadi, S. Sahmani, "Bending, buckling and free vibration analysis of size-dependent functionally graded circular/annular microplates based on the modified strain gradient elasticity theory", *Eur. J. Mech. A/Solids* **49** (2015), p. 251-267.

[22] S. Sahmani, R. Ansari, "On the free vibration response of functionally graded higher-order shear deformable microplates based on the strain gradient elasticity theory", *Compos. Struct.* **95** (2013), p. 430-442.

[23] N. C. Tho, N. T. Thanh, T. D. Tho, P. Van Minh, L. K. Hoa, "Modelling of the flexoelectric effect on rotating nanobeams with geometrical imperfection", *J. Braz. Soc. Mech. Sci. Eng.* **43** (2021), no. 11, article no. 510.

[24] H. X. Nguyen, T. N. Nguyen, M. Abdel-Wahab, S. P. A. Bordas, H. Nguyen-Xuan, T. P. Vo, "A refined quasi-3D isogeometric analysis for functionally graded microplates based on the modified couple stress theory", *Comput. Methods Appl. Mech. Eng.* **313** (2017), p. 904-940.

[25] M. Bahreman, H. Darijani, A. Bahrani Fard, "The size-dependent analysis of microplates via a newly developed shear deformation theory", *Acta Mech.* **230** (2019), no. 1, p. 49-65.

[26] Y. S. Li, E. Pan, "Static bending and free vibration of a functionally graded piezoelectric microplate based on the modified couple-stress theory", *Int. J. Eng. Sci.* **97** (2015), p. 40-59.

[27] M. Kandaz, H. Dal, "Finite element analyses of the modified strain gradient theory based Kirchhoff microplates", *Surfaces* **4** (2021), no. 2, p. 115-156.

[28] M. H. Ghayesh, H. Farokhi, M. Amabili, "Nonlinear dynamics of a microscale beam based on the modified couple stress theory", *Compos. B: Eng.* **50** (2013), p. 318-324.

[29] M. Asghari, "Geometrically nonlinear micro-plate formulation based on the modified couple stress theory", *Int. J. Eng. Sci.* **51** (2012), p. 292-309.

[30] Y.-G. Wang, W.-H. Lin, C.-L. Zhou, "Nonlinear bending of size-dependent circular microplates based on the modified couple stress theory", *Arch. Appl. Mech.* **84** (2014), no. 3, p. 391-400.

[31] W.-Y. Jung, W.-T. Park, S.-C. Han, "Bending and vibration analysis of S-FGM microplates embedded in Pasternak elastic medium using the modified couple stress theory", *Int. J. Mech. Sci.* **87** (2014), p. 150-162.

[32] K. Foroutan, H. Ahmadi, "Nonlinear static and dynamic buckling analyses of imperfect fgp cylindrical shells resting on nonlinear elastic foundation under axial compression", *Int. J. Struct. Stab. Dyn.* **20** (2020), no. 7, article no. 2071005.

[33] B. Zhang, Y. He, D. Liu, L. Shen, J. Lei, "An efficient size-dependent plate theory for bending, buckling and free vibration analyses of functionally graded microplates resting on elastic foundation", *Appl. Math. Model.* **39** (2015), no. 13, p. 3814-3845.

[34] Y. Yang, Y. Dong, Y. Li, "Buckling of piezoelectric sandwich microplates with arbitrary in-plane BCs rested on foundation: effect of hygro-thermo-electro-elastic field", *Eur. Phys. J. Plus* **135** (2020), no. 1, article no. 61.

[35] Q. Li, D. Wu, W. Gao, F. Tin-Loi, Z. Liu, J. Cheng, "Static bending and free vibration of organic solar cell resting on Winkler–Pasternak elastic foundation through the modified strain gradient theory", *Eur. J. Mech. - A/Solids* **78** (2019), article no. 103852.

[36] A. Gupta, M. Talha, "Static and stability characteristics of geometrically imperfect FGM plates resting on pasternak elastic foundation with microstructural defect", *Arab. J. Sci. Eng.* **43** (2018), no. 9, p. 4931-4947.

[37] B. Bouderba, "Bending of FGM rectangular plates resting on non-uniform elastic foundations in thermal environment using an accurate theory", *Steel Compos. Struct.* **27** (2018), no. 3, p. 311-325.

[38] L. M. Thai, D. T. Luat, V. B. Phung, P. Van Minh, D. Van Thom, "Finite element modeling of mechanical behaviors of piezoelectric nanoplates with flexoelectric effects", *Arch. Appl. Mech.* **92** (2022), no. 1, p. 163-182.

[39] C. Wu, J. Lou, L. He, J. Du, H. Wu, "Buckling and post-buckling of symmetric functionally graded microplate lying on nonlinear elastic foundation based on modified couple stress theory", *Int. J. Struct. Stab. Dyn.* **18** (2018), no. 09, article no. 1850110.

[40] M. Sobhy, A. M. Zenkour, "A comprehensive study on the size-dependent hygrothermal analysis of exponentially graded microplates on elastic foundations", *Mech. Adv. Mater. Struct.* **27** (2020), no. 10, p. 816-830.

[41] Q. Li, D. Wu, W. Gao, F. Tin-Loi, "Size-dependent instability of organic solar cell resting on Winkler–Pasternak elastic foundation based on the modified strain gradient theory", *Int. J. Mech. Sci.* **177** (2020), article no. 105306.

[42] V.-K. Tran, T.-T. Tran, M.-V. Phung, Q.-H. Pham, T. Nguyen-Thoi, "A finite element formulation and nonlocal theory for the static and free vibration analysis of the sandwich functionally graded nanoplates resting on elastic foundation", *J. Nanomater.* **2020** (2020), article no. 8786373.

[43] T. T. Tran, V. K. Tran, P. B. Le, V. M. Phung, V. T. Do, H. N. Nguyen, "Forced vibration analysis of laminated composite shells reinforced with graphene nanoplatelets using finite element method", *Adv. Civ. Eng.* **2020** (2020), article no. 1471037.

[44] T. Q. Bui, D. H. Doan, T. Van Do, S. Hirose, N. D. Duc, "High frequency modes meshfree analysis of Reissner–Mindlin plates", *J. Sci. Adv. Mater. Devices* **1** (2016), no. 3, p. 400-412.

[45] M. Van Phung, D. T. Nguyen, L. T. Doan, D. Van Nguyen, T. Van Duong, "Numerical investigation on static bending and free vibration responses of two-layer variable thickness plates with shear connectors", *Iran. J. Sci. Technol. - Trans. Mech. Eng.* (2022).

[46] A. Tessler, T. J. R. Hughes, "An improved treatment of transverse shear in the mindlin-type four-node quadrilateral element", *Comput. Methods Appl. Mech. Eng.* **39** (1983), no. 3, p. 311-335.

[47] T. J. Ypma, "Historical development of the Newton–Raphson method", *SIAM Rev.* **37** (1995), no. 4, p. 531-551.

[48] N. T. Hong, "Nonlinear static bending and free vibration analysis of bidirectional functionally graded material plates", *Int. J. Aerosp. Eng.* **2020** (2020), article no. 8831366.